

Metamaterials-based terahertz sensor for quick diagnosis of early lung cancer

Xin Xu (胥欣)^{1,4}, Yan Wu (吴艳)², Tangyan He (何唐艳)², Yuanyuan Li (李媛媛)^{1,4},
Fangrong Hu (胡放荣)^{1,4,*}, Huasheng Liang (梁华晟)², Chunxia Yang (杨春霞)³,
and Hong Zhong (钟宏)³

¹College of Electronic Engineering and Automation, Guilin University of Electronic Technology, Guilin 541004, China

²Beihai Endocrinology Institute, the Ninth Affiliated Hospital of Guangxi Medical University, Beihai 536000, China

³Department of Thoracic Surgery, the Ninth Affiliated Hospital of Guangxi Medical University, Beihai 536000, China

⁴Guangxi Experiment Center of Information Science, Guilin 541004, China

*Corresponding author: hufangrong@sina.com

Received July 10, 2017; accepted September 4, 2017; posted online September 20, 2017

We experimentally demonstrate a metamaterials (MMs)-based terahertz (THz) sensor to quickly distinguish the cancer tissues from normal tissues. The MMs-based THz sensor has two strong resonance absorption peaks at about 0.706 and 1.14 THz, respectively. When the sensor is covered with cancer tissues, the redshifts at about 0.706 and 1.14 THz are 31 and 19 GHz, respectively. However, if normal tissue is attached to the surface of the sensor, the corresponding redshifts are only 15 and 12 GHz, respectively. This study proposes a new method for quick diagnosis of early lung cancer and other cancers.

OCIS codes: 170.6510, 300.6495.

doi: 10.3788/COL201715.111703.

Due to the fact that the blood supply and water content in cancer tissues are more than those in normal tissues, and terahertz (THz) spectrum is very sensitive to the change of water content, THz technology can be applied to the diagnosis and detection of cancers^[1]. Bowman *et al.* successfully distinguished breast cancer areas from normal areas using THz imaging technology, and the method can also be applied to very thin dehydration isomer samples^[2]. Oh *et al.* obtained the reflection image of a rat glioma and clearly detected its boundary^[3], which is very useful for studying brain lesions and structure. Yamaguchi *et al.* studied the fresh brain tumor tissues of a rat, calculated the refractive index and absorption coefficient of cancer and normal tissues, and got a two-dimensional (2D) scan image^[4]. Their results indicated that it is feasible to use the THz technology to detect brain tumors. Moreover, compared with conventional magnetic resonance imaging (MRI) and the fluorescence imaging method, THz imaging technology can distinguish the fuzzy boundary more clearly. Hou found that there is an obvious difference between THz absorption spectrum of gastric cancer tissues and that of normal tissues^[5]. In addition, using the relationship between the optical properties of human skin and the blood glucose^[6], Cherkasova created a THz non-contact method for the diagnosis of diabetes.

Currently, lung cancer has become one of the most malignant tumors hazardous to human health, and more than one million people die from lung cancer each year^[7]. Although the technologies for diagnosis and treatment of lung cancer have made significant progress, its mortality is still very high. The main reason is that early lung cancer has no symptoms and is very difficult to be exactly diagnosed by general diagnosis methods, including

bronchoscopy, mediastinoscopy, biopsy, pleural effusion cytology, thoracotomy biopsy and exploration, etc. Moreover, the general methods are very complicated or time consuming. Therefore, quick diagnosis of early lung cancer is of great significance at present.

Metamaterials (MMs)^[8,9] are artificial composite materials and structures that have special physical properties, such as negative index, electromagnetic stealth, and super absorption. A THz sensor based on MMs is sensitive to the change of the dielectric covered on its surface, and, thus, it can find wide applications in biomedicine. Tao *et al.*^[10] made MM THz split-ring resonators (SRRs)^[11] on different substrates to study their sensing properties and found that the SRRs on the ultra-thin silicon nitride substrate show higher sensitivity and more superior performance. Wu *et al.* used the SRRs to characterize the reaction process of streptavidin agarose^[12]. In addition, the MMs with Fano^[13] or multipolar resonances^[14] are useful for THz sensors.

In this Letter, we designed and fabricated an MM-based THz sensor to help quickly distinguish early lung cancer tissues from the normal tissues.

As shown in Fig. 1(a), the unit cell of the MMs sensor consists of an inner aluminum circle and an outside aluminum Ohm ring on the high resistance silicon substrate. Its geometrical parameters are $R_1 = 16 \mu\text{m}$, $R_2 = 20 \mu\text{m}$, $R_3 = 24 \mu\text{m}$, $R_4 = 30 \mu\text{m}$, $g = 8 \mu\text{m}$, and $w = 74 \mu\text{m}$. The thicknesses of the aluminum and silicon substrates are 0.1 and 350 μm , respectively. The THz wave is polarized along the y axis and normally incident to the top surface of the sensor. Simulation is completed using commercialized software CST Microwave Studio 2015. In the simulation, an open boundary condition is set in the

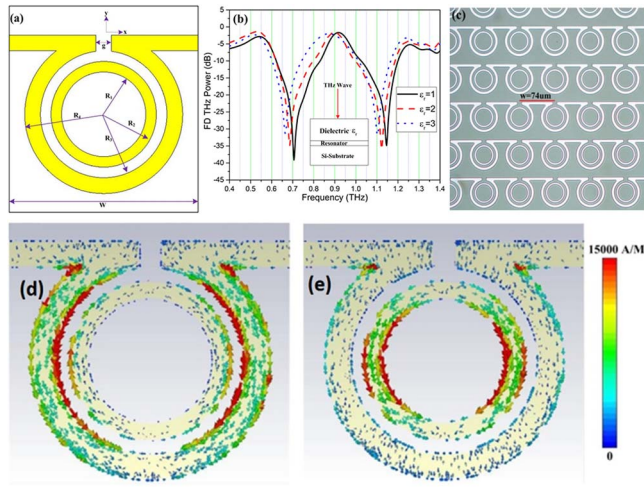


Fig. 1. (Color online) (a) Top view of a unit cell, (b) transmission spectra, (c) micrograph of the sample, (d) surface currents distributions at 0.706 and (e) 1.14 THz.

z direction, and the unit cell boundary condition is set in the x and y directions. Aluminum film is modeled as lossy metal with an electrical conductivity^[15] $\sigma = 3.57 \times 10^7$ S/m. A high resistance silicon substrate is modeled as a normal material with an electrical conductivity^[15] $\sigma = 2.5 \times 10^{-4}$ S/m and a relative dielectric constant^[15] $\epsilon_r = 11.9$. Figure 1(b) shows the transmission spectra of the sensor covered with different dielectrics. When $\epsilon_r = 1$, which means the surface of the sensor is only covered with air, there are two resonance absorption peaks locating at $f_1 = 0.706$ THz and $f_2 = 1.14$ THz, respectively. When the surface of sensor is covered with a 100- μm -thick medium with a relative permittivity of $\epsilon_r = 2$ or 3, the corresponding resonance peaks show a distinct redshift, and the frequency shift increases with the increase of the relative permittivity. This indicates that the sensor is sensitive to the change of the dielectric. The micrograph of the sample is shown in Fig. 1(c), and its whole size is about 9 mm \times 9 mm. The distributions of the surface currents at 0.706 and 1.14 THz are calculated and illustrated in Figs. 1(d) and 1(e), respectively.

Figures 1(d) and 1(e) show that the surface current of 0.706 THz mainly oscillates on the left and right arms of the outside Ohmic ring, and that of 1.14 THz mainly oscillates on the inner circle. They are of a typical electrical dipole resonance. Therefore, the resonance absorption peak at about 0.706 THz is produced by the outside Ohmic ring, and that of 1.14 THz is induced by the inner circle.

A Z-3 model THz time-domain spectroscopy (TDS) system is used to test the samples. The tissues, i.e., the normal tissue and cancer tissue, are taken from the patient, who has been diagnosed with early lung cancer by the general method.

First, as shown in Fig. 2(a), two kinds of tissues with the same thickness of 100 μm are adhered to a 650- μm -thick plastic. The THz time-domain (TD) and frequency-domain

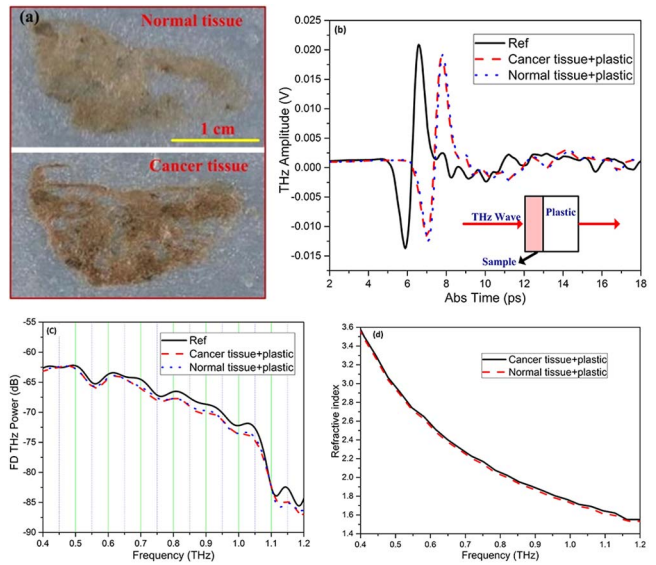


Fig. 2. (Color online) (a) Photograph of normal tissue and cancer tissue, (b) THz TD spectra, (c) THz FD spectra, and (d) refractive index curve.

(FD) transmission spectrum of them are obtained and plotted in Figs. 2(b) and 2(c), respectively. The black solid line is the reference spectrum of air. The red dotted line is the spectrum of the composite structure of cancer tissue and plastic, and the blue dotted line is the spectrum of the composite structure of normal tissue and plastic.

Figure 2(b) shows that the spectrum of the composite structure with cancer tissue almost has the same delay time as that with normal tissue. Therefore, these two kinds of tissues cannot be distinguished by the TD spectrum. Figure 2(c) shows that the composite structure with the cancer tissue has a low amplitude, and the probable reason is because the blood supply and water content in cancer tissues are more than those in normal tissues. The dips in the FD spectra are mainly resulted from the absorption of water.

In addition, the refractive index is usually used to distinguish the samples. The refractive index $n(\omega)$ of the sample can be calculated as follows^[16]:

$$n(\omega) = \frac{\Phi(\omega)c}{\omega d} + 1, \quad (1)$$

where ω is frequency, c is the velocity of light in vacuum, and d is the thickness of the sample. The phase $\Phi(\omega)$ can be obtained from fast Fourier transform of the TD spectrum. The $n(\omega)$ calculated from Eq. (1) is plotted in Fig. 2(d).

Figure 2(d) shows that the refractive index of the cancer tissue is a little larger than that of the normal tissue. The probable reasons are (1) cancer tissues contain more water, and (2) cancer cells have a large nucleus, large density, thick film, etc.

Although, we can distinguish the cancer tissue from normal tissue by comparing their refractive indexes, it

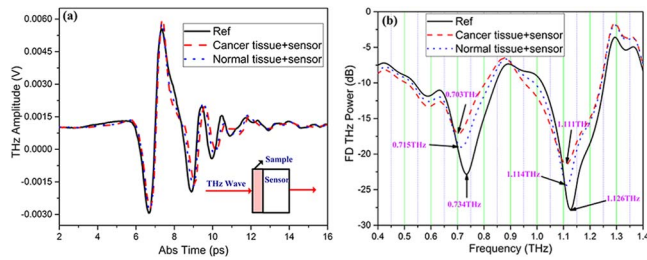


Fig. 3. (Color online) (a) Measured THz TD spectrum and (b) FD spectrum.

is complicated and time consuming. Moreover, for early lung cancer, the refractive index of the cancer tissue is very close to that of normal tissue. Therefore, this method is not effective and easy to misdiagnose.

In order to solve this problem, we introduce an MMs-based THz sensor to quickly diagnose early lung cancer.

In our experiment, the transmission of the sensor without tissue is first measured as a reference. After that, a piece of early lung cancer tissue and a piece of normal tissue with the same thickness of 100 μm are separately adhered to the top surface of the sensor. The measured THz TD spectra and FD spectra are shown in Figs. 3(a) and 3(b), respectively.

Figure 3 shows that, compared with the reference without tissues, the sensor with tissues shows a distinct redshift. At the low frequency absorption peak, the sensor with cancer tissue produces a redshift of 31 GHz, while the sensor with normal tissue only yields a redshift of 19 GHz. In addition, at the high frequency absorption peak, the sensor with cancer tissues shows a distinct redshift of 15 GHz, and normal tissues only generated a 12 GHz redshift.

The probable reason for the redshift is that when the tissues adhered to the surface of MMs-based THz sensor the equivalent dielectric constants on the surface increases. The MMs-based THz sensor is very sensitive to the change of the dielectric constants on the surface. The more the equivalent dielectric constant is, the larger the redshift is.

Due to the refractive index $n (= \sqrt{\epsilon\mu})$ of the cancer tissue that is larger than that of the normal tissue, the equivalent dielectric constant of the cancer tissue is consequently larger than that of the normal tissue. Thus, the sensor covered with cancer tissue shows a larger redshift than that covered with normal tissue, and this can be used to distinguish the cancer tissues from the normal tissues.

In conclusion, we design an MMs-based THz sensor to quickly diagnose early lung cancer. The sensor has two

strong absorption peaks located at 0.706 and 1.14 THz, which are very sensitive to the change of the dielectric constant on the surface. When the sensor is covered with cancer tissues, the redshifts at a low frequency and at a high frequency are 31 and 19 GHz, respectively. However, the corresponding redshifts for normal tissue are only 15 and 12 GHz, respectively. Compared with the conventional method of calculating the refractive index of the samples, the method based on the MMs THz sensor is quick, simple, and label free. Therefore, it is very effective for quickly diagnosing early lung cancer, whose refractive index is very close to that of normal tissue. The method presented in this Letter is still effective for quickly diagnosing of many other cancers.

This work was supported by the National Natural Science Foundation of China (No. 11574059), the Natural Science Foundation of Guangxi (Nos. 2015GXNSFDA19039 and 2014GXNSFAA118376), and the Foundation from Guangxi Key Laboratory of Automatic Detection Technology and Instrument (No. YQ14114).

References

1. A. Rahman, A. K. Rahman, and B. Rao, *Biosens. Bioelectron.* **82**, 64 (2016).
2. T. C. Bowman, M. El-Shenawee, and L. K. Campbell, *IEEE Trans. Antennas Propag.* **63**, 2088 (2015).
3. S. J. Oh, S. H. Kim, and Y. B. Ji, *Biomed. Opt. Express* **5**, 2837 (2014).
4. S. Yamaguchi, Y. Fukushi, and O. Kubota, *Phys. Med. Biol.* **61**, 3638 (2016).
5. D. Hou, X. Li, and J. Cai, *Phys. Med. Biol.* **59**, 5423 (2014).
6. O. P. Cherkasova and M. M. Nazarov, *Bull. Russ. Acad. Sci. Phys.* **80**, 479 (2016).
7. J. Hu, G. S. Qian, and C. X. Bai, *Cancer* **121**, 3157 (2015).
8. Z. Li, C. Luo, and F. Ling, *Chin. Opt. Lett.* **14**, 102303 (2016).
9. Z. Yang, F. Gao, and Y. Hou, *Chin. Opt. Lett.* **14**, 061602 (2016).
10. H. Tao, A. C. Strikwerda, and M. Liu, *Appl. Phys. Lett.* **97**, 261909 (2010).
11. Q. Wu, F. Lan, Y. Zhang, and X. Gao, *Chin. Opt. Lett.* **13**, 101601 (2015).
12. X. Wu, B. Quan, and X. Pan, *Biosens. Bioelectron.* **42**, 626 (2013).
13. L. Chen, N. Xu, L. Singh, T. Cui, R. Singh, Y. Zhu, and W. Zhang, *Adv. Opt. Mater.* **5**, 1600960 (2017).
14. L. Chen, Y. M. Wei, X. F. Zang, Y. M. Zhu, and S. L. Zhuang, *Sci. Rep.* **6**, 22027 (2016).
15. www.cst.com/Content/Products/MWS/Overview.aspx.
16. E. F. Patz, Jr., P. C. Goodman, and G. Beple, *N. Engl. J. Med.* **343**, 1627 (2000).